Article

Insights into the Nature of the Active Sites of Pt-WO$_x$/Al$_2$O$_3$ Catalysts for Glycerol Hydrogenolysis into 1,3-Propanediol

Clara Jarauta-Córdoba [1], Mikel Oregui Bengoechea [2], Iker Agirrezabal-Telleria [2], Pedro-Luis Arias [2] and Iñaki Gandarias [2,*]

[1] Centro de Investigación de Recursos y Consumos Energéticos (CIRCE), 50018 Zaragoza, Spain; cajarauta@fcirce.es

[2] Department of Chemical and Environmental Engineering, School of Engineering, University of the Basque Country (UPV/EHU), 48013 Bilbao, Spain; mikel.oregui@ehu.eus (M.O.B.); iker.aguirrezabal@ehu.eus (I.A.-T.); pedroluis.arias@ehu.eus (P.-L.A.)

* Correspondence: inaki.gandarias@ehu.eus; Tel.: +34-94-6017373

Abstract: The chemo-selective hydrogenolysis of secondary hydroxyls is an important reaction for the production of biomass-derived α,ω-diols. This is the case for 1,3-propanediol production from glycerol. Supported Pt-WO$_x$ materials are effective catalysts for this transformation, and their activity is often related to the tungsten surface density and Brönsted acidity, although there are discrepancies in this regard. In this work, a series of Pt-WO$_x$/γ-Al$_2$O$_3$ catalysts were prepared by modifying the pH of the solutions used in the active metal impregnation step. The activity–structure relationships, together with the results from the addition of in situ titrants, i.e., 2,6-di-tert-butyl-pyridine or pyridine, helped in elucidating the nature of the bifunctional active sites for the selective production of 1,3-propanediol.

Keywords: glycerol; 1,3-propanediol; tungsten oxide; platinum; Brönsted acid; α,ω-diols

1. Introduction

A common property of biomass-derived building blocks, such as sugars, polyols and cyclic ethers, is their relatively high O/C ratio. Hence, catalytic C-O hydrogenolysis reactions are interesting routes for the valorization of these building blocks into value-added chemicals with lower O/C ratios [1]. For instance, α,ω-diols, which have a linear carbon chain and hydroxy groups at both terminal positions, are widely used commodity chemicals in polyesters and polyurethane resin production [2]. Currently, most of the α,ω-diols are industrially obtained through petrochemical routes. Nonetheless, the chemo-selective C-O hydrogenolysis of cyclic ethers and polyols constitutes a promising alternative to producing them from biomass feedstock. This is the case for 1,5-pentanediol production from tetrahydrofurfuryl alcohol [3], 1,6-hexanediol from tetrahydropyran-2-methanol [4] or 1,3-propanediol (1,3-PDO) from glycerol [5]. This last transformation has attracted an enormous amount of interest from the scientific community, due to the large glycerol surplus generated by the biodiesel industry [6] and the high demand for 1,3-PDO as a raw material in polytrimethylene terephthalate production.

Selective 1,3-PDO production is a remarkable challenge, as glycerol hydrogenolysis can also yield 1,2-propanediol (1,2-PDO). The hydrogenolysis of a primary C-O bond, which leads to 1,2-PDO, is favored with catalytic systems based on copper and nickel [7–9]. The selective hydrogenolysis of the secondary C-O bond requires a special class of bi-functional heterogeneous catalysts, based on the combination of a precious metal, i.e., Pt, Ir or Rh, and an oxophilic metal, such as rhenium or tungsten [10]. As of the time of writing, the best 1,3-PDO yields have been reported with Pt-WO$_x$ catalytic systems, using ZrO$_2$ or alumina supports [11].

The activity of Pt-WO$_x$/Al$_2$O$_3$ catalysts towards 1,3-PDO follows a volcano shape with respect to the tungsten content, with negligible 1,3-PDO production in the absence of the oxophilic metal (i.e., Pt/Al$_2$O$_3$) catalyst [5]. As the tungsten content increases in the catalyst, higher 1,3-PDO yields are obtained, until a maximum is reached for an optimum level of tungsten content. Above this value, the 1,3-PDO yield decreases with the amount of tungsten. This behavior is related to the different tungsten species that appear in the catalyst surface as a function of the tungsten surface density (ρW): at low coverage, mono-tungstates are predominant; at medium ρW values, polytungstates are favored, while WO$_3$ nanocrystals appear at higher surface coverage [5]. For a γ-Al$_2$O$_3$ support, the maximum tungsten surface density before the appearance of WO$_3$ nanocrystals (ρW^{lim}) is below the theoretical monolayer content [12–14]. Among the three species, the polytungstates are considered the active ones for chemo-selective glycerol hydrogenolysis into 1,3-PDO [14–16]. However, there is not yet a consensus on their role in the reaction mechanism.

Some groups have reported a direct correlation between the number of Brønsted acid sites and the 1,3-PDO yield in Pt-WO$_x$-based catalytic systems [17–19]. Moreover, the optimum tungsten surface density ρW^{opt} matches the ρW^{lim} at which the polytungstates are maximized [16]. Under H$_2$ pressure, and in the presence of a precious metal, H$^{\delta+}$(WO$_3$)$_n$$^{\delta-}$ type Brønsted sites are formed via the local reduction of polytungstate domains [20]. On the contrary, monotungstates or WO$_3$ nanocrystals are not capable of delocalizing the negative charge required to stabilize H$^{\delta+}$ species. Nonetheless, some other groups did not find a clear correlation between the Brønsted acidity and the 1,3-PDO yield when using Pt/WO$_x$ catalytic systems [14,15], and the ρW^{opt} was below the ρW^{lim}.

In this study, the effect that the pH of the solutions containing the metal precursors has on the structure, activity and selectivity of the Pt-WO$_x$/Al$_2$O$_3$ catalytic system was determined. These results, together with the study of in situ titrants, i.e., 2,6-di-*tert*-butyl-pyridine or pyridine, were used to gain insights into the nature of the bifunctional active sites leading to the selective hydrogenolysis of glycerol into 1,3-PDO. The stability study of Pt nanoparticles and polytungstates in the aqueous-phase reaction environment [21,22] was beyond the scope of this article.

2. Results

The adsorption mechanism of metal ions on oxide surfaces can be explained by an electrostatic model controlled by the isoelectric point (IEP) of the oxide, the pH of the impregnation solution and the charge of the metal complex [23]. At a pH above the IEP of the oxide, the surface is negatively charged and cations are attracted and bound electrostatically to the surface. On the contrary, at a pH bellow the IEP, anions are drawn from the solution to the positively charged surface. In the case of the catalytic system under study, the IEP of the oxide surfaces is around 7.5 for the γ-Al$_2$O$_3$ [24] and around 6 in the case of the 10W/Al$_2$O$_3$ [25]. Regarding the precursors, the Pt is in the form of a cation, [Pt(NH$_3$)$_4$]$^{2+}$, while tungsten is in the form of an oxyanion, [H$_2$W$_{12}$O$_{40}$]$^{6-}$.

2.1. Effect of the pH Value of the Platinum Impregnation Solution

For bifunctional Pt-WO$_x$/γ-Al$_2$O$_3$ catalysts, a close interaction between Pt and the polytungstates is required in order to selectively produce the desired 1,3-PDO [5]. Herein, we analyzed whether these interactions could be tuned by controlling the pH of the solution containing the platinum precursor. First, 10 wt.% tungsten on alumina material was prepared following the first sequential impregnation step described in the experimental section (pH = 8.5). Next, a series of four catalysts were prepared by impregnating 5 wt.% of Pt at pH values of 4, 6, 8 and 10. These catalysts are denoted as xPt^{pH}yW, where 'x' refers to the theoretical Pt content (wt.%) in the final catalyst and 'y' to the W content related to the γ-Al$_2$O$_3$ support.

As can be observed in Table 1, entries 1–4, the pH of the impregnating solution did not have a significant influence on the platinum particle size. The dispersion values, estimated through the CO chemisorption technique, were around 30% for all samples. The most

relevant effect was related to the Pt loading achieved, i.e., 3.5 wt.%, when the impregnation pH was below the IEP of the $10W/Al_2O_3$ material (pH = 4 vs IEP $\approx$ 6). Under these conditions, the surface of the oxide is positively charged and, therefore, the adsorption of the Pt cations is not electrostatically favored [26].

Table 1. Composition and dispersion data for different $Pt\text{-}WO_x/Al_2O_3$ catalysts.

Entry	Catalyst/ $\gamma\text{-}Al_2O_3$	W (wt%) [1]	Pt (wt%) [1]	Pt Dispersion (%) [2]	Pt Size (nm) [2]
1	$5Pt^{pH4}10W$	9.0	3.5	30.8	3.0
2	$5Pt^{pH6}10W$	9.2	4.3	25.1	3.8
3	$5Pt^{pH8}10W$	9.1	4.3	25.9	3.6
4	$5Pt^{pH10}10W$	9.3	4.3	30.5	3.1
5	$5Pt^{pH10}10W$ *	9.9	4.6	29.4	3.2
6	$5Pt^{pH10}15W$ *	14.6	4.9	21.2	4.4
7	$5Pt^{pH10}20W$ *	18.3	4.6	15.5	6.1
8	$2.5Pt^{pH10}15W$ *	14.2	2.5	27.9	3.4
9	$10Pt^{pH10}15W$ *	13.4	8.6	22.2	4.3

[1] Determined by ICP. [2] Determined by CO chemisorption of reduced samples. * Tungsten impregnation was carried out at pH 1.5.

The XPS measurements of the same four samples (Table 2, entries 1–4) show that the Pt/Al surface ratios were very close to the Pt/Al bulk ratios (obtained by ICP-AES), confirming the good dispersion of the Pt. The binding energies (315.4–315.8 eV) of the Pt $4d_{5/2}$ spectral region indicate that Pt was in the form of PtO [27]. The W/Al surface ratios were also close to the bulk values. This result agrees with the homogenously dispersed mono- and polytungstate structures, with no nanocrystal formation. Moreover, the fact that all the samples had the same W/Al surface ratios indicates that the pH did not affect the Pt anchoring sites on the $WO_x/\gamma\text{-}Al_2O_3$ surface.
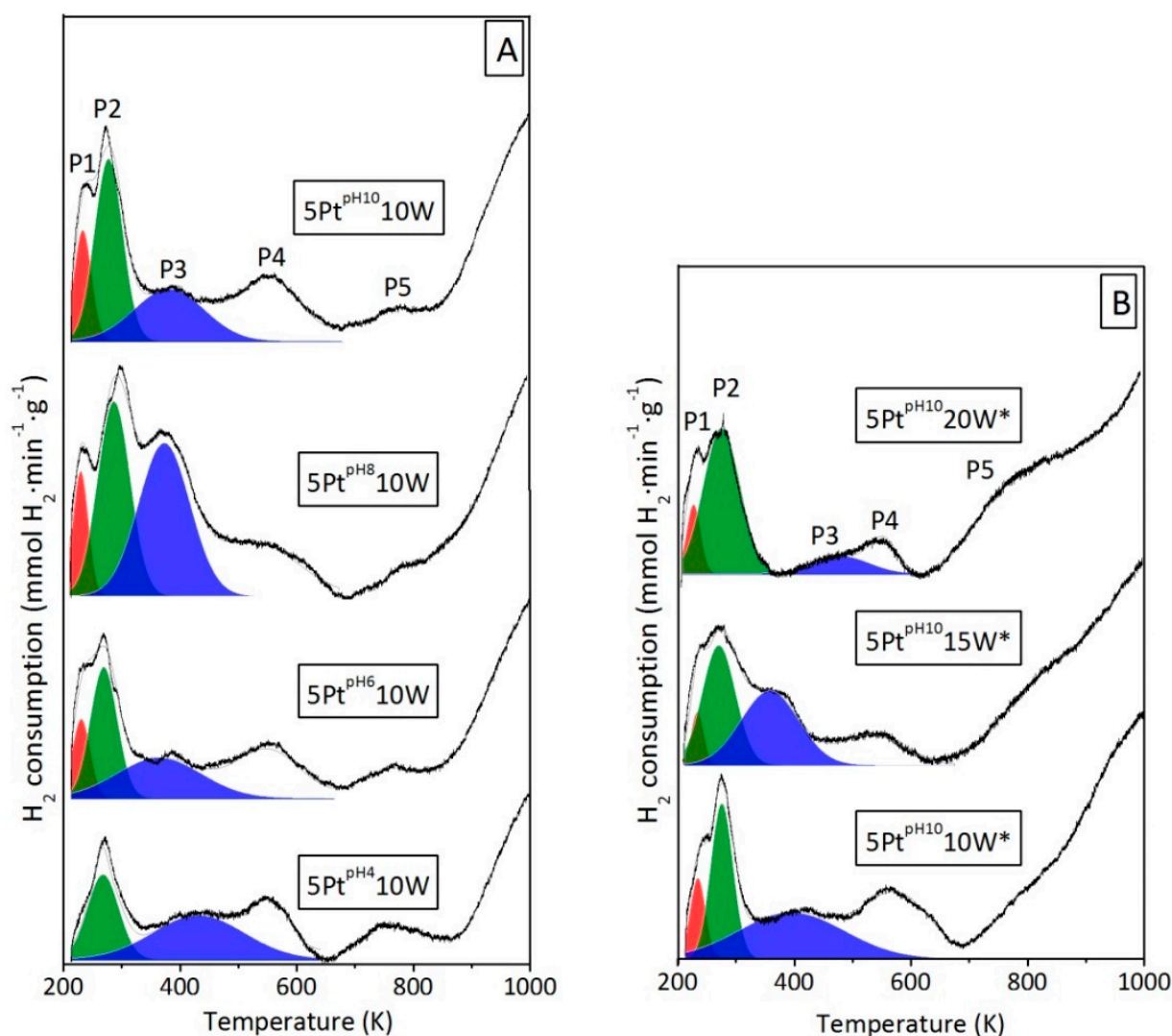
Table 2. Bulk atomic ratio obtained from ICP-AES, surface atomic ratio obtained from XPS and binding energies (BE) of the Pt and W elements for calcined $Pt\text{-}WO_x/Al_2O_3$ catalysts.

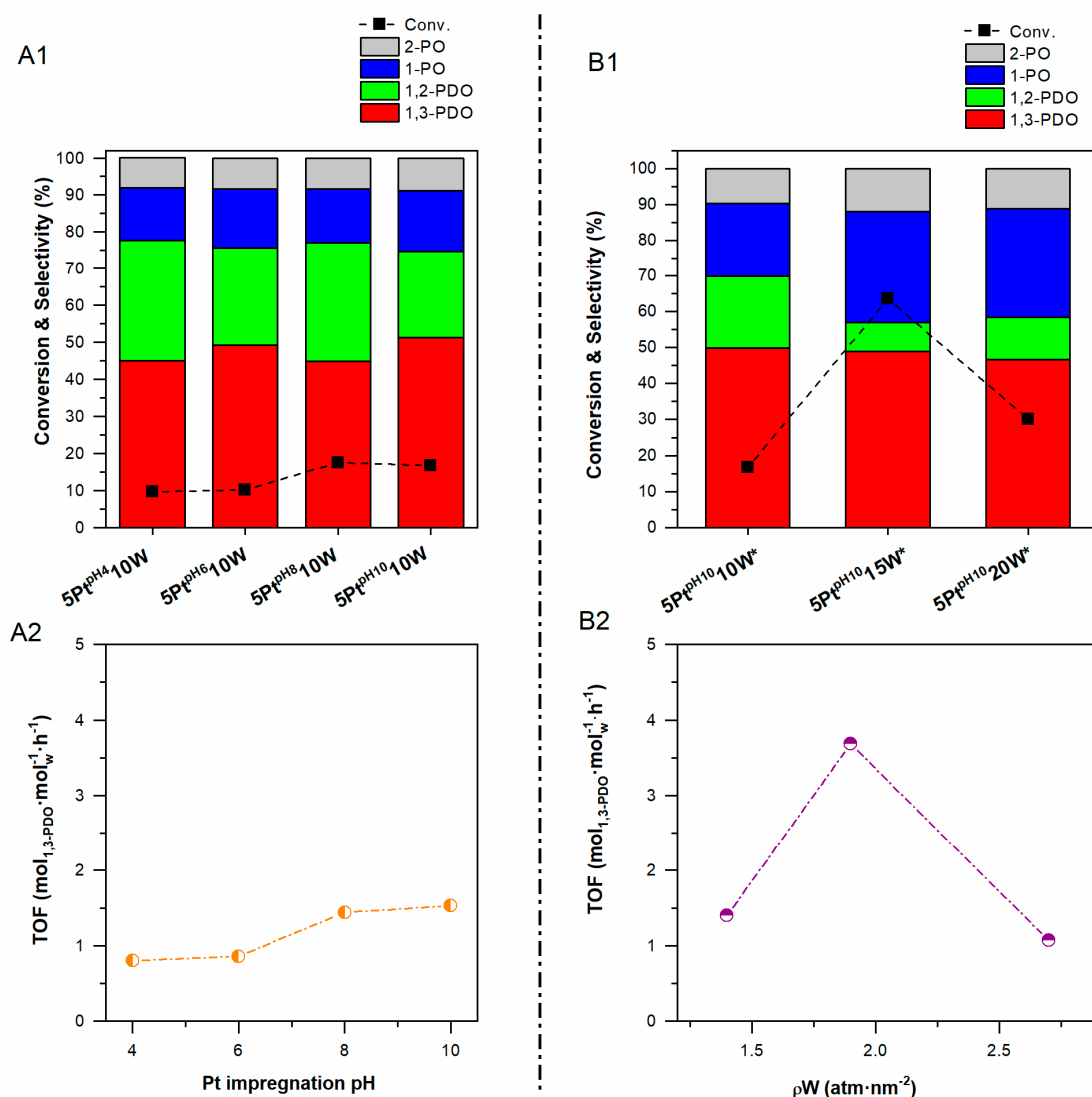| Entry	Sample	Pt/Al		W/Al		BE (eV)	
		Bulk	Surface	Bulk	Surface	Pt $4d_{5/2}$	W $4f_{7/2}$
1	$5Pt^{pH4}10W$	0.009	0.011	0.021	0.022	315.5	35.4
2	$5Pt^{pH6}10W$	0.010	0.012	0.022	0.023	315.5	35.5
3	$5Pt^{pH8}10W$	0.010	0.013	0.020	0.023	315.6	35.5
4	$5Pt^{pH10}10W$	0.010	0.012	0.020	0.023	315.8	35.6
5	$5Pt^{pH10}10W$ *	0.010	0.010	0.024	0.029	315.6	35.4
6	$5Pt^{pH10}15W$ *	0.012	0.011	0.037	0.041	315.4	35.4
7	$5Pt^{pH10}20W$ *	0.011	0.011	0.049	0.063	315.5	35.3

* Tungsten impregnation was carried out at pH 1.5.

Similar TPR profiles were recorded for the four samples (Figure 1A). The two hydrogen consumption peaks at subambient temperatures (T < 278 K) are related to the reduction of Pt^{2+} species showing different reducibility. It has been reported that the interaction of platinum and tungsten oxide species on alumina supports generates more reducible $Pt^{\delta+}$ species [28]. Hence, the lowest temperature peak is assigned to those platinum species highly interacting with the polytungstates. In the case of the catalyst in which the platinum is impregnated at pH 4, the lowest temperature reduction peak is less evident, which points to a lower $Pt\text{-}WO_x$ interaction. The third hydrogen consumption peak (T between 363–431 K) might correspond to the reduction of bulk PtO species with low interaction with the polytungstates. Nonetheless, the amount of hydrogen corresponding to the first three peaks exceeds the required theoretical one to reduce all the platinum present in the samples (see Table S1). Part of the H_2 consumption could be a consequence of the hydrogen spillover, which occurs even at room temperature in these types of catalytic systems [20]. The reduction of WO_3

occurs in three steps: $WO_3 \rightarrow WO_{2.9} \rightarrow WO_2 \rightarrow W$ [29]. The first reduction step occurs at temperatures around 700 K, or lower if Pt is present [20]. Hence, the fourth and fifth hydrogen consumption peaks correspond to the $WO_3 \rightarrow WO_{2.9}$ reduction step, with and without Pt interaction, respectively. For the sample impregnated at pH 4, the fifth peak is significantly higher than for the other samples. This, again, indicates a lower Pt-WO_x interaction when a pH lower than the IEP is used. Finally, the hydrogen consumption at temperatures above 873 K corresponds to the further $WO_{2.9} \rightarrow WO_2 \rightarrow W$ reduction.

Figure 1. H_2-TPR profiles for different Pt/WO_x/Al_2O_3 catalysts. Effect of the Pt impregnation pH (**A**) and the W impregnation pH (**B**). The * symbol refers to the pH value of 1.5 during tungsten impregnation.

The four 5Pt^{pH4-10}10W catalysts were tested in the glycerol hydrogenolysis reaction. The Pt impregnation pH did not significantly affect the product selectivity, the glycerol conversion or the activity towards 1,3-PDO (Figure 2, left). The fact that the highest $TOF_{1,3-PDO-W}$ was obtained for the catalyst in which the Pt was impregnated at the largest pH is ascribed to the slightly better Pt dispersion obtained under these conditions, since a negative charge surface favors Pt cation impregnation. In summary, the pH at which the Pt is impregnated does not notably affect the Pt dispersion or the Pt-WO_x interactions. For this reason, similar $TOF_{1,3-PDO-W}$ values were obtained regardless of the pH.

Figure 2. Performance of Pt-WO$_x$/γ-Al$_2$O$_3$ catalysts in glycerol hydrogenolysis. Left: Effect of the Pt impregnation pH on glycerol conversion and product selectivity (**A1**), and on TOF$_{1,3\text{-PDO-W}}$ (**A2**). Right: Effect of the ρW on glycerol conversion and product selectivity (**B1**), and on TOF$_{1,3\text{-PDO-W}}$ (**B2**). Operating conditions: 473 K, 55 MPa H$_2$, 5 wt.% glycerol water solution, 0.3 g$_{cat}$·g$_{glycerol}^{-1}$, 4 h.

2.2. Effect of the pH Value of the Tungsten Impregnation Solution

As described in the Introduction, polytungstates are the most active tungsten species for the selective transformation of glycerol into 1,3-PDO. They are predominant at intermediate tungsten surface densities, as, above certain tungsten density values (ρW^{lim}), WO$_3$ nanocrystals appear. When the pH of the tungsten impregnation solution was 8.5, nanocrystals appeared for tungsten content levels higher than 10 wt.% (ρW^{lim} ≈ 1.3 at. nm^{-2}). Bulk WO$_3$ crystallites are visually identified by their light yellow color, in contrast to the well-dispersed white polytungstantes (see Figure S1 for 10W/Al$_2$O$_3$ and 15W/Al$_2$O$_3$ materials). There are different strategies to increase the tungsten loading at which the nanocrystals start appearing, e.g., increasing the BET area of the support [16] or adding promoters, such as Li$_2$B$_4$O$_7$ [19] or phosphorous [30], to hinder the migration and aggregation of surface tungsten oxides. Another approach is to control the pH of the solution. Based on previous works [30], we decided to impregnate the tungsten at pH 1.5. Under these conditions, the

alumina support is positively charged, which favors the adsorption of anions, and the tungstate oxyanions' equilibrium is shifted towards the poly-oxometalate [31]:

$$12WO_4^{-2} + 12H^+ \Leftrightarrow 6H_2O + W_{12}O_{42}^{12-} \tag{1}$$
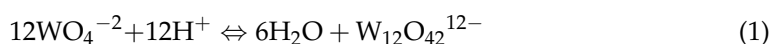
A series of $WO_x/\gamma\text{-}Al_2O_3$ materials were prepared at pH = 1.5 and tungsten content between 10 and 30 wt.%. These materials are denoted as $yW*$, where 'y' refers to the W content and * to the pH value of 1.5 during the tungsten impregnation. Raman spectra of the calcined materials (see Figure 3) revealed that crystalline WO_3 bands (ca. 800, 700 and 270 cm^{-1}) [32] only appeared for tungsten loadings above 20 wt.%. Hence, by reducing the impregnation pH from 8.5 to 1.5, the ρW^{lim} value almost doubled (1.3 vs. 2.7 at. nm^{-1}), indicating that a low pH value limits the aggregation of well-dispersed tungsten oxide species. All the samples showed a band near 970 cm^{-1}, which is attributed to the W = O vibration mode characteristic of mono- and polytungstate species [33]. Nonetheless, the intensity of this band was lower for those samples containing WO_3 nanoparticles (i.e., 25W* and 30W*), which correlates with a lower proportion of polytungstates.
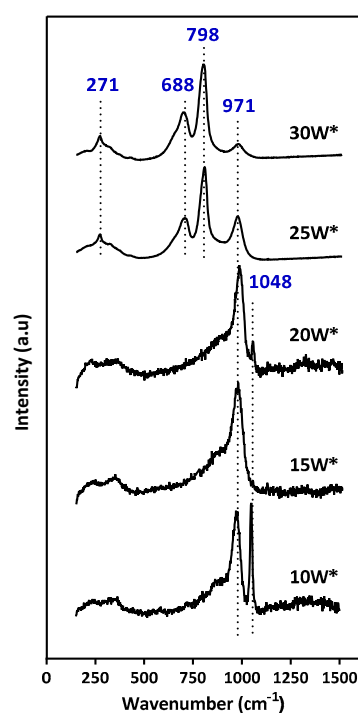
Figure 3. Raman spectra for different tungsten oxide $\gamma\text{-}Al_2O_3$ materials impregnated at pH 1.4. The * symbol refers to the pH value of 1.5 during tungsten impregnation.

Based on the Raman results, 5 wt.% of Pt was impregnated on the three $WO_x/\gamma\text{-}Al_2O_3$ materials prepared at pH 1.5, which did not show the appearance of nanocrystals (i.e., 10, 15 and 20 wt.% of tungsten). These catalysts are denoted as $5Pt^{pH10}yW*$.

The data in Table 1 (entries 5–7) show that the Pt dispersion decreased with the tungsten loading. This indicates that, as the polytungstate domain increases, some of the PtO anchoring sites on the support are occupied or less accessible, which leads to a poorer Pt distribution after reduction. Kwak et al. [34] observed that PtO anchors at specific Al^{3+} sites on a bare $\gamma\text{-}Al_2O_3$ support. The analysis of XPS results (Table 2, entries 5–7) indicates that Al^{3+} sites are also the preferential sites for PtO on the $WO_x/\gamma\text{-}Al_2O_3$ surface, as the Pt BE does not change with the tungsten loading. Furthermore, the surface W/Al atomic ratio linearly increases with tungsten loading for the $5Pt^{pH10}10W*$, $5Pt^{pH10}15W*$ and $5Pt^{pH10}20W*$ catalysts, which correlates with the good dispersion of tungsten when it is in the form of mono- and polytungstates.

The activity of the 5Pt$^{\text{pH10}}$yW* (y = 10, 15 or 20) in glycerol hydrogenolysis was also evaluated. The 5Pt$^{\text{pH10}}$10W* catalyst gave very similar conversion and 1,3-PDO selectivity values compared to the 5Pt$^{\text{pH10}}$10W (Figure 2). Therefore, for a similar tungsten content level, the pH at which the tungsten is impregnated does not significantly affect the activity or selectivity of the catalysts. On the contrary, the tungsten content, or the ρW, had a notable influence on the glycerol conversion and on the activity of the catalyst towards 1,3-PDO. The TOF$_{\text{1,3-PDO-W}}$ increased three-fold when the tungsten content was raised from 10 to 15%, and decreased sharply when it was further augmented to 20%. Interestingly, the highest activity towards the secondary hydroxy group hydrogenolysis, 1,3-PDO, was not obtained for the catalyst containing the highest amount of tungsten content before the appearance of tungsten nanocrystals, but at an optimum tungsten surface density below this value: ρW$^{\text{opt}}$ (1.93 at $_{\text{w}}$·nm^{-2}) < ρW$^{\text{lim}}$ (2.71 at $_{\text{w}}$·nm^{-2}). In order to check whether this activity trend was maintained for other diols, the same three catalysts were tested in the hydrogenolysis of 1,2-PDO and 1,2-butanediol (1,2-BDO). With these reactants, 1-propanol (1-PO) and 1-butanol (1-BO) are formed, respectively, after the hydrogenolysis of the secondary hydroxy group. Results (Figure S2) show that, regardless of the substrate, the catalyst showing the highest activity towards the secondary hydroxyl bond hydrogenolysis was 5Pt$^{\text{pH10}}$15W*.

To determine whether the acidity properties correlate with the large variation in the TOF$_{\text{1,3-PDO-W}}$ values as a function of the catalyst ρW, NH$_3$-TPD measurements of the tungstated supports were carried out (Figure S3). The NH$_3$ desorption signal was divided into three regions: weak sites (T < 473 K), medium sites (473–623 K) and strong sites (623–723 K). The signal above the catalyst calcination temperature (T > 723 K) was not considered, as the thermal stability of the material is not warranted. For all the tungstated supports, the acid amount displayed the following trend: weak acid > medium acid > strong acid (see Table S2). Moreover, the ρW does not significantly affect the total acidity, or the strength distribution, although the catalyst with the highest tungsten loading (i.e., 20W*) presents the largest amount of strong acid sites.

In order to differentiate between the Lewis and Brønsted acid sites, FTIR spectra of pyridine adsorption were generated (see Figure 4). Lewis sites interacting with pyridine (LPy) produce signals at 1615, 1495 and 1450 cm^{-1}, while Brønsted sites (BPy) show signals at 1630 and 1540 cm^{-1}. Finally, physisorbed pyridine (PPy) appears at 1600 and 1580 cm^{-1} [35]. In order to determine the Brønsted to Lewis ratio (B/L), the integration area of the absorbance peaks at 1540 and 1450 cm^{-1} was utilized for Brønsted and Lewis sites, respectively. The integration results, shown in Table S2, show that the Lewis acidity is predominant for all the materials, and that only the material with the largest amount of tungsten, i.e., 20W*, presents prominent Brønsted acidity. For all the samples, the B/L ratio slightly increases with the vacuum treatment temperature. As can be observed in Figure S4, for all the samples, more than 60% of the area related to Lewis sites and more than 70% of the area related to Brönsted sites remained after the highest vacuum treatment temperature (573 K) was applied. These results indicate that both types of acid sites present weak, medium and strong sites, although the latter are more predominant for the Brönsted type. The fact that the catalyst with the ρW$^{\text{lim}}$ presents the strongest Brønsted acidity is in line with other works that point to the necessity of an extended polytungstate network to delocalize the negative charge required to generate H$^{\delta+}$(WO$_3$)$_n^{\delta-}$ sites [20].

The acidity results of yW*/γ-Al$_2$O$_3$ materials do not show a relationship between the number of Brønsted sites and the activity of the corresponding Pt-yW*/γ-Al$_2$O$_3$ catalysts towards 1,3-PDO. It was not possible to measure the B/L ratio of the catalysts containing Pt, because, at temperatures higher than 523 K, pyridine is easily reduced to piperidine on the reduced catalysts, which causes difficulties for spectra analysis. The H$^{\delta+}$(WO$_3$)$_n^{\delta-}$ site generation is promoted by Pt metal sites under a H$_2$ atmosphere. Therefore, a different B/L ratio under the operating conditions compared to the FTIR conditions cannot be excluded. Moreover, the reaction takes place in the aqueous phase, which might also affect the acidity properties of the catalysts.
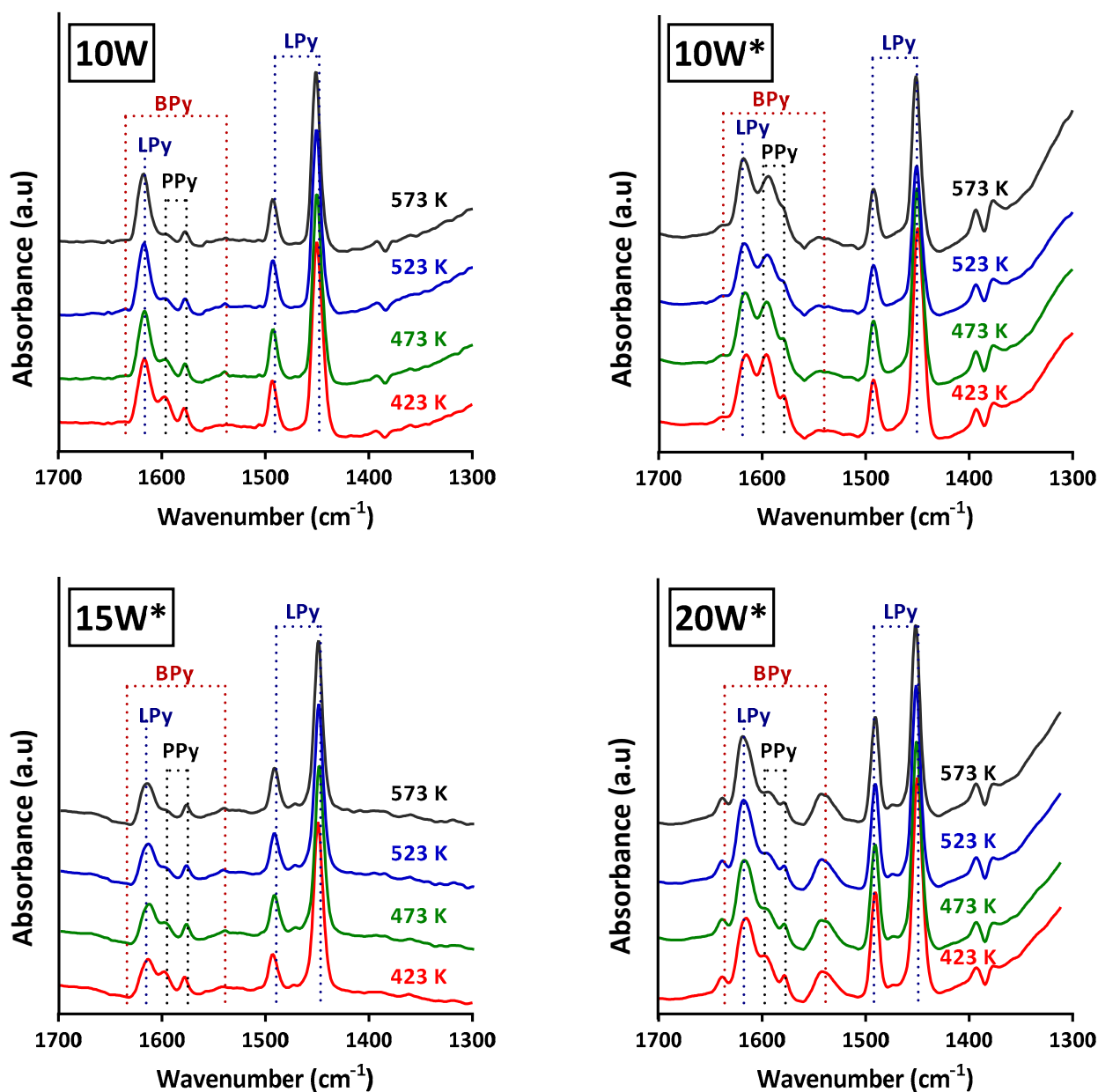
Figure 4. FTIR spectra of adsorbed pyridine measured after vacuum treatments at different temperatures for different tungsten oxide γ-Al$_2$O$_3$ materials. The * symbol refers to the pH value of 1.5 during tungsten impregnation.

In order to clarify the role of Brønsted and Lewis sites, activity tests for glycerol hydrogenolysis were carried out, adding in situ titrants, such as 2,6-di-*tert*-butyl-pyridine (which only adsorbs on Brønsted sites) and pyridine (which adsorbs on both Brønsted and Lewis sites). In each experiment, 0.20 mmol of titrant was added, which was, in principle, sufficient to titrate the 0.13 mmol of acid sites present in 0.15 g of catalyst (estimated from TPD-NH$_3$ measurements). As observed in Figure 5, no 1,3-PDO formation was observed when pyridine was used as the titrant, which means that Lewis acid sites are mandatory for the formation of the α,ω-diol. Notably, significant 1,3-PDO production was measured when adding 2,6-di-*tert*-butyl-pyridine, and the TOF$_{1,3\text{-PDO-W}}$ was only reduced by less than one third (ca. 30%) compared to the activity test with no titrant. Hence, under our reaction conditions, 1,3-PDO could be obtained even in the absence of Brønsted sites in the catalyst.
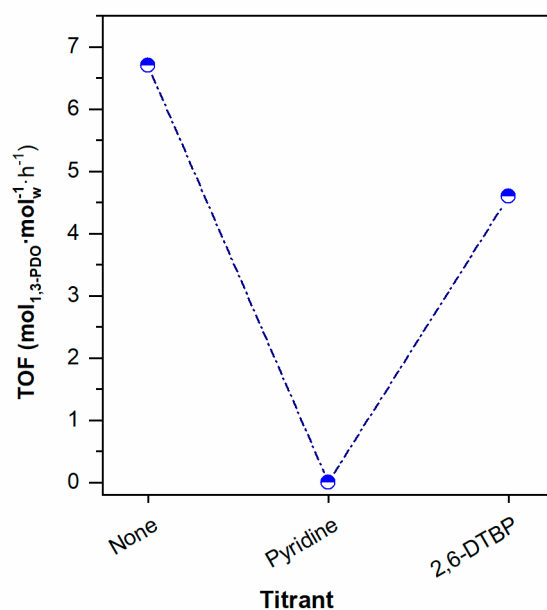
Figure 5. For the $10Pt^{pH10}15W^*$ catalysts, effect of the presence of a titrant (i.e., pyridine or 2,6-di-tert-butyl-pyridine) in the $TOF_{1,3\text{-PDO-W}}$. Operating conditions: 473 K, 55 MPa H_2, 5 wt.% glycerol water solution, 0.3 $g_{cat} \cdot g_{glycerol}^{-1}$.

In summary, impregnating tungsten over a γ-Al_2O_3 support at a pH value of 1.5 allows an increase in the ρW^{lim} (the maximum tungsten surface density before nanocrystals appears) as compared to impregnation at pH 8.5. The material with the ρW^{lim} value (20W*) showed the highest acidity and Brønsted to Lewis ratio. Nonetheless, when Pt was incorporated, the $5Pt^{pH10}15W^*$ catalyst showed almost three-fold higher $TOF_{1,3\text{-PDO-W}}$ than the $5Pt^{pH10}20W^*$. Hence, and as previously observed by other authors [14,15], for our catalytic system, $\rho W^{opt} < \rho W^{lim}$, and there is no direct relationship between Brønsted acidity and the 1,3-PDO yield.

2.3. Effect of Pt Site Availability

Another possible hypothesis to explain why $\rho W^{opt} < \rho W^{lim}$ for the Pt-WO_x/Al_2O_3 catalytic system is the necessity of a compromise between Pt sites (or dispersion for catalysts with the same Pt content) that decrease with ρW and glycerol anchoring sites (polytungstates) that increase with ρW. The results given in Section 2.1. show that modifying the pH of the Pt impregnation solution is not the best technique to increase the Pt dispersion. Therefore, in order to check for the effect of Pt site availability, catalysts with the same support, $15W^*/\gamma$-Al_2O_3, and different Pt content levels (i.e., 2.5, 5 and 10 wt.%) were prepared.

For this series, the Pt dispersion decreases with increasing loading from 2.5 to 5 wt.%, and then it remains stable (Table 1, entries 6, 8 and 9). The activity tests with these catalysts were carried out at different reaction times (1–4 h) in order to obtain similar glycerol conversion values (15–22%) for all the catalysts. At these conditions, secondary hydrogenolysis conditions, leading to 1-propanol and 2-propanol, are minimized. As observed in Figure 6A, the $TOF_{1,3\text{-PDO-W}}$ increases linearly with the amount of active Pt in the catalysts, for materials with the same $15W^*/\gamma$-Al_2O_3 support. Hence, for the same ρW, which means a similar type and amount of polytungstates, the catalyst activity towards 1,3-PDO and the Pt dispersion are directly related. On the contrary, if we compare the $TOF_{1,3\text{-PDO-W}}$ and the amount of active Pt for catalysts with different ρW (Figure 6A), the linear relationship is lost. In fact, the $2.5Pt^{pH10}15W^*$ catalyst presents a slightly lower amount of Pt sites than the $5Pt^{pH10}20W^*$, but its $TOF_{1,3\text{-PDO-W}}$ is almost twice as high. These results indicate that the tungsten oxide active sites are different for catalysts with different ρW, even if no WO_3 nanoparticles are formed. Moreover, the nature of these

tungsten species has a higher influence on 1,3-PDO production than the amount of Pt sites (or Pt dispersion for catalysts with the same Pt content). The latter is only relevant for catalysts with the same tungstated support.
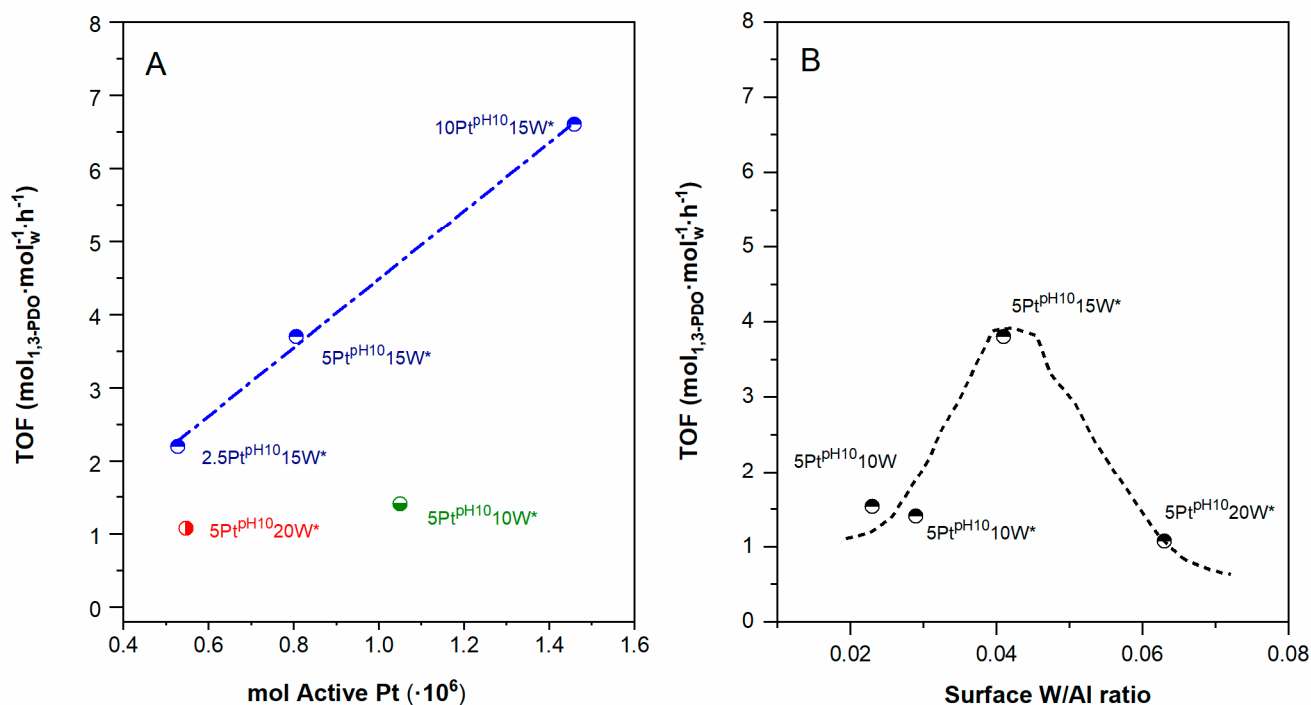
Figure 6. (**A**) Correlation between $TOF_{1,3\text{-PDO-W}}$, obtained at similar conversion values (15–20%), and mol of active Pt present in the reaction, for catalysts presenting different Pt and/or W contents. (**B**) For catalysts with 5 wt.% Pt impregnated at pH 10, effect of the surface W/Al ratio (determined by XPS). Operating conditions: 473 K, 55 MPa H_2, 5 wt.% glycerol water Scheme 0. $g_{cat} \cdot g_{glycerol}^{-1}$. The * symbol refers to the pH value of 1.5 during tungsten impregnation.

2.4. Effect of the Alumina Surface Coverage

A third possible explanation as to why $\rho W^{opt} < \rho W^{lim}$ is related to the work by Aihara et al. [14,36], who proposed that the active sites for glycerol adsorption are at the boundary between the polytungstates and the alumina: W-(OH)-Al sites.

It is clear that, below the monolayer coverage, the larger the tungsten content, the higher the alumina coverage, and hence a lower amount of aluminum sites would be exposed to the surface. This can be observed in Table 2, which shows that, as expected, the W/Al ratio increases with tungsten loading. In Figure 6B, the $TOF_{1,3\text{-PDO-W}}$ follows a volcano shape for catalysts with the same Pt content, with respect to the W/Al ratio, suggesting that, for the Pt-WO$_x$/Al$_2$O$_3$ catalytic system, there might be an optimum level of alumina coverage.

3. Discussion

Previously presented results indicate that, when using a cationic precursor, impregnating the platinum at a pH value higher than the IEP of the tungstated support has a minor positive effect on the Pt dispersion and on the $TOF_{1,3\text{-PDO-W}}$. On the contrary, when impregnating tungsten using an oxyanion, low pH values (pH < IPE) promote the formation of polytungstates and increase the ρW^{lim} value before the appearance of nanoparticles. Nonetheless, a direct correlation between Brønsted acidity and the 1,3-PDO yield was not observed, and the ρW^{opt} was lower than the ρW^{lim}. The reason for this was not the availability of Pt active sites (Section 2.3), as the 2.5Pt^{pH10}15W* and the 5Pt^{pH10}20W* presented a similar amount of Pt active sites, but the $TOF_{1,3\text{-PDO-W}}$ of the former was almost doubled. Pt availability is only relevant for catalytic materials with the same tungstated support

(similar ρW). Interestingly, the results given in Section 2.4 show that there is an optimum W/Al ratio, suggesting that the alumina might also play a role in active site formation.

　　　For a better understanding of the nature of the active sites, it is convenient to focus on the reaction mechanism. It is widely accepted that the formation of 1,3-PDO from glycerol occurs through a direct hydrogenolysis mechanism in which the first step is the adsorption of glycerol on a polytungstate site to form a primary alkoxide. After this step, previous works [5,17] suggest a proton → hydride mechanism (Scheme 1a). A carbocation is formed after the protonation–dehydration of the secondary hydroxy group. Next, a hydride generated on a nearby platinum site attacks this secondary carbocation and releases the target product.

a) Proton-hydride mechanism

b) Hydride-proton mechanism
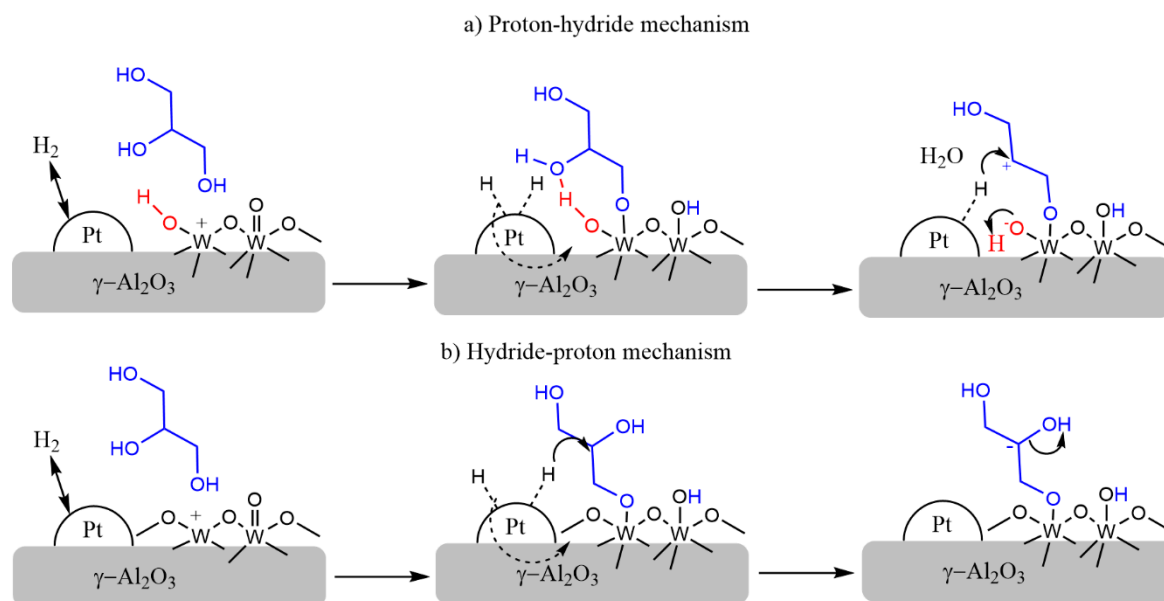
Scheme 1. Model structures of the transition states for the proton–hydride mechanism (**a**) and for the hydride–proton mechanism (**b**).

　　　However, our results point to a different reaction mechanism for the Pt-WOx/γ-Al$_2$O$_3$ catalytic system. Firstly, in this and other works [15,16], a relationship between Brønsted acidity and 1,3-PDO yield was not observed. Secondly, a prominent TOF$_{1,3\text{-PDO-W}}$ was obtained when 2,6-di-*tert*-butyl-pyridine was added to the reaction media. These results suggest that the protonation step is not the rate-determining one.

　　　For an Ir-ReO$_x$/SiO$_2$ catalytic system, Tomishige's group [37] proposed another mechanism that occurs via an anion intermediate, formed after the regioselective attack of a hydride to the 2-position of the alkoxide to break the C-O bond (hydride → proton mechanism). The structure–activity results shown in our work highlight the hydride transfer as the rate-limiting step also for the Pt-WOx/γ-Al$_2$O$_3$ catalytic system (see Scheme 1b). The three main pieces of evidences are as follows: (i) for the same tungstated support, there is a linear correlation between the amount of Pt active sites (where hydrides are formed) and TOF$_{1,3\text{-PDO-W}}$; (ii) we previously reported [15] a first order in hydrogen pressure, i.e., hydrogen availability, in 1,3-PDO production using Pt-WO$_x$/γ-Al$_2$O$_3$ materials; (iii) the reaction takes place at a significant rate, even in the absence of Brønsted acidity in the catalyst. This last piece of experimental evidence indicates that protonation is not the rate-limiting step, and that the release of the reduced alkoxide can also take place through a hydrolysis step in the aqueous medium.

　　　Taking all into account, we propose that the bifunctional active sites would be formed by closely interacting (i) W $^{\delta+}$-O-Al sites at the boundary between the polytungstates and the alumina, for the adsorption and activation of glycerol, and (ii) Pt sites for the activation of hydrogen. This active site configuration can explain why the optimum ρW^{opt} is below ρW^{lim}. The presence of an Al atom in the active site would modulate, to an optimum value,

the adsorption strength of the adsorbed alkoxide. Hence, there is a critical tungsten surface density, ρW^{opt}, in which a compromise is achieved between: (i) large surface coverage of polytungstates, which increases the ability of WO_x domains to undergo slight reduction, and (ii) a large number of $W^{\delta+}$-O-Al sites at the boundary between the polytungstates and the alumina. Above the ρW^{opt}, some of the $W^{\delta+}$-O-Al sites are converted into less active $W^{\delta+}$-O-W sites.

Further experimental results using in situ titrants and spectroscopic techniques should be carried out to confirm the suggested hydride–proton mechanism and the bifunctional active sites.

4. Materials and Methods

4.1. Catalyst Synthesis

Pt-WO_x/Al_2O_3 catalysts were prepared by a sequential wetness impregnation method. γ-Al_2O_3 (*Alfa Aesar* $\geq$ 99.9 wt.%) was used as a support, while ammonium metatungstate ((NH_4)$_6$($H_2W_{12}O_{40}$)·nH_2O, *Sigma Aldrich-Merck* $\geq$ 99.99 wt.%) and tetraammineplatinum (II) (Pt(NH3)4(NO3)2 nitrate, *Sigma Aldrich-Merck* $\geq$ 99.995 wt.%) were used as W and Pt precursors, respectively. Ammonia (NH_3, 25 wt.%, *Panreac*) and nitric acid (HNO_3, 65 wt.% technical grade, *Panreac*) were used to adjust the pH value during the impregnation step. The synthesis procedure is detailed below.

First, the tungsten precursor was impregnated on the γ-Al_2O_3 support. Appropriate amounts of ammonium metatungstate, to obtain the required theoretical W content in the sample, were dissolved in ultra-pure water. Next, the commercial γ-Al_2O_3 support was added (9:1 g_{water}:$g_{\gamma\text{-}Al2O3}$) and the resulting slurry (pH 8.5) was stirred at room temperature for 1 h. In some preparations, the pH of the tungsten impregnation solution was set to 1.5, by adding appropriate amounts of HNO_3 and NH_3. The solvent surplus was removed under vacuum in a rotary evaporator (*Heidolph Laborota 4000 efficient*) at 333 K. Impregnated samples were dried at 383 K overnight and calcined in flowing air from room temperature up to 723 K at a heating rate of 2 K·min^{-1}. This temperature was held for 4 h. The second step was the impregnation of the Pt precursor on the supported tungsten oxide materials. Required amounts of tetraammineplatinum (II) nitrate were dissolved in ultra-pure water, the supported tungsten oxide material was added (9:1 g_{water}:$g_{support}$), and the suspension was stirred for 1 h. Different pH values for the Pt impregnation solution were tested (i.e., 4, 6, 8 and 10), following the previously mentioned procedure. The resulting catalysts were dried as above and calcined at 573 K.

The prepared Pt-WO_x/γ-Al_2O_3 catalysts are denoted as xPt^{pH}yW, where 'x' refers to the theoretical Pt content (wt.%) in the final catalyst and 'y' to the W content related to the γ-Al_2O_3 support. The different pH values set during the Pt impregnation are indicated in the '*pH*' superscript. When the impregnation of the W precursor was carried out at pH 1.5, the samples were denoted as xPt^{pH}yW*.

The tungsten surface density (expressed in W atoms·nm^{-2} of supported tungsten oxide samples) was calculated based on the following equation:

$$\rho W \ (\text{atm W·nm}^{-2}) = \frac{\left(\frac{x_w}{M_w}\right) \cdot N_A}{S_{sample}/\left(1 - x_{WO_3}\right)} \tag{2}$$

where X_W is the mass fraction of the W species in the final catalyst, N_A is the Avogadro number, M_W is the W atomic weight, and S_{sample} is the BET surface area of the calcined supported tungsten oxide samples. In order to calculate X_{WO3}, it was assumed that all the tungsten oxide species present in the catalyst were in the form of WO_3. The ρW values for each material are shown in Table S3.

4.2. Catalyst Characterization

4.2.1. Chemical Analysis

The chemical analysis of the catalysts was carried out by inductively coupled plasma atomic emission spectroscopy (ICP-OES), using a Perkin Elmer Optima 2000 instrument. Prior to the chemical analysis, the solid samples were digested in a microwave oven (Ethos1, Milestone) in a mixture of HF, HCl and HNO_3, by heating from room temperature to 453 K for 30 min.

4.2.2. N_2 Physisorption

The textural properties were determined by N_2 physisorption at 77 K, using an AUTOSORB-1C-TCD instrument (Quantachrome Instruments). In order to remove the residual humidity or organic species, all the samples were outgassed at 673 K for 5 h under high vacuum, prior to the physisorption measurements. The surface area was calculated using the Brunauer, Emmett and Teller (BET) method and the pore size distributions were obtained by the Barrett–Joyner–Halenda (BJH) method, applied to the desorption branch of the isotherms. The BET area and pore volume of the supported tungsten oxide samples are presented in Table S3.

4.2.3. CO Chemisorption

The metallic dispersion and the Pt particle size were determined by CO chemisorption, using an AutoChem II instrument (Micromeritics, Norcross, GA, USA). The catalysts were in-situ-reduced at 673 K under a 50 cm^3STP/min flow of 5 vol.% H_2/He. Subsequently, the samples were evacuated under He flow for 1 h and then cooled down to 303 K. Finally, CO chemisorption uptake was measured at 303 K with pulses of 5 vol.% CO/He.

4.2.4. Raman Spectroscopy

The different WO_x species present in the catalysts (monotungstates, polytungstates and/or WO_3 nanocrystals) were determined by Raman spectroscopy, using an InVia microscope (Renishaw) equipped with an Ar ion laser (Modue-Laser), using 514 nm laser excitation. The spectra were recorded at ambient temperature within the 150–1500 cm^{-1} region.

4.2.5. XPS

XPS spectra of the calcined samples were recorded in order to determine the Pt oxide species. The analyses were performed in a SPECS instrument equipped with a Phoibos 150 1D-DLD energy analyzer and an AlK_α (*hν* = 1486.7 eV) Focus 500 monochromatic radiation source. The recorded XPS signals were analyzed using a nonlinear Shirley-type background and decomposed into subcomponents by Gaussian–Lorentzian functions.

4.2.6. NH_3-TPD

The catalysts' acidity was quantified by NH_3-TPD in an AutoChem II instrument (Micromeritics, Norcross, GA, USA). The samples were firstly pretreated at 548 K under He flow for 1 h, in order to remove residual humidity or adsorbed species. Next, reduction took place under hydrogen flow from room temperature to 573 K. Subsequently, the samples were cooled down in He flow and then NH_3-saturated at 373 K using a 5 cm^3STP/min flow of 0.5 vol.% NH_3/He. Physisorbed NH_3 was removed from the catalyst surface by flowing He for 1 h. Finally, NH_3 desorption was performed by increasing the temperature up to 1073 K, while recording simultaneously the TCD signal.

4.2.7. FTIR of Adsorbed Pyridine

The nature of the acid sites of supported tungsten oxide samples was determined by FTIR of adsorbed pyridine. A VERTEX 70 spectrometer (Bruker, Karlsruhe, Germany) and an external sample compartment (XSA) were used. The samples were pretreated following different stages, prior to pyridine exposure. First, they were heated under a vacuum (10^{-3} mbar) at 573 K for 1 h to remove any organic species present on the surface.

Next, they were reduced at 573 K under hydrogen flow. After cooling down the system, vacuum conditions were set and the samples were exposed to pyridine for 10 min. Finally, several heating cycles of 15 min in a vacuum at different temperatures (423, 473, 523 and 673 K) were carried out, to determine the strength of the acid sites. After each heating cycle, the spectra were recorded at 313 K.

Measurements were taken in the whole spectrum range, using 200 scans and a 4 cm^{-1} resolution, although only results from the 1700–1300 cm^{-1} region, where Lewis and Brønsted signals appear, are shown (Figure 4).

4.3. Activity Tests

The activity tests were carried out in a 50 mL stainless steel batch reactor (RWTH Aachen Universität, Aachen, Germany). Prior to the activity tests, the catalyst was ex-situ-reduced in a tubular oven under a stream of pure hydrogen (100 mL·min^{-1}) at 673 K, 5 K·min^{-1} heating rate and 1 h isotherm. After the reduction, the catalyst was kept in *n-hexane* to avoid oxidation. Before each experiment, *n-hexane* was evaporated and 0.15 g of the dry catalyst powder (0–500 μm) was introduced into a glass liner, which was placed into the stainless steel reactor. The reactant solution (10 g of an aqueous 5 wt.% glycerol solution), was placed into the same liner together with a magnetic stirrer. The reactor was then closed, purged three times with H$_2$, pressurized up to 5.5 MPa of hydrogen and placed on the pre-heated plates. The reaction temperature was set at 473 K under a stirring rate of 550 rpm. A standard activity test lasted 4 h. Tests at different reaction times were also carried out to obtain TOFs at similar conversion values. Titration experiments were performed for 30 min, by adding 100 μL of pyridine or 2,6-di-*tert*-butyl-pyridine to the reactant solution.

After the required reaction time, the reactor was cooled down to room temperature without stirring. After opening the reactor, a known amount of 1,4-butanediol (Sigma–Aldrich, 99.99%) was added to the reactor as an internal standard, and the liquid sample was analyzed with a gas chromatograph (Agilent Technologies, 7890 A) equipped with a flame ionization detector (FID) and a thermal conductivity detector (TCD). The conversion of glycerol, the selectivity of the liquid products and the TOF values were calculated based on the following equations:

$$\text{Conversion (\%)} = \frac{\sum \text{mol of all liquid products}}{\text{mol of reactant in the feeding}} \cdot 100 \quad (3)$$

$$\text{Selectivity (\%)} = \frac{\text{mol of the liquid product}}{\text{mol of all liquid products}} \cdot 100 \quad (4)$$

$$\text{TOF (mol}_{\text{product}} \cdot \text{mol}_w^{-1} \cdot h^{-1}) = \frac{\text{mol of product}}{\text{mol of W in the catalyst} \cdot \text{reaction time}} \quad (5)$$

5. Conclusions

The pH of the Pt impregnation solution does not significantly affect the Pt dispersion or the Pt-WO$_x$ interactions. Therefore, similar TOFs$_{1,3\text{-PDO-W}}$ were obtained regardless of the pH. On the contrary, by reducing the impregnation pH of the tungsten precursor solution from 8.5 to 1.5, the tungsten surface density value before the appearance of WO$_3$ nanoparticles doubled (1.3 vs. 2.7 at. nm^{-1}). Hence, a low pH value, below the IEP of the γ-Al$_2$O$_3$, limits the aggregation of well-dispersed tungsten oxide species. The catalyst with the largest amount of polytungstates (20 wt.% of tungsten) showed the highest Brønsted to Lewis ratio; nonetheless, its activity towards the secondary bond hydrogenolysis was lower compared to the catalysts with lower tungsten content. The same activity trend was obtained when using 1,2-PDO or 1,2-BDO as reactants.

Activity tests using in situ titrants showed that Lewis sites are more relevant than Brønsted sites for the selective production of 1,3-PDO. Based on activity and characterization

results, a bifunctional active site is proposed, formed by closely interacting W $^{\delta+}$-O-Al sites, for the adsorption and activation of glycerol, and Pt sites for the activation of hydrogen.

Supplementary Materials: The following are available online at https://www.mdpi.com/article/10.3390/catal11101171/s1. Figure S1: Visual identification of bulk WO3 crystallites (of yellow color) on the 15W/γ-Al2O3 material (right). The 10W/γ-Al2O3 material (left) is shown for comparison, Figure S2: Correlation between TOFproduct-W and tungsten surface density for 5PtpH10yW* catalysts. 1-propanol (1-PO) and 1-butanol (1-BO) are the products obtained after the hydrogenolysis of the secondary hydroxyl group, when 1,2-propanediol (1,2-PDO) or 1,2-butanediol (1,2-BDO) are used as substrate; Figure S3: TPD-NH3 profiles for different tungsten oxide γ-Al2O3 materials; Table S1: Ratio between the H2 consumption in peaks related to the PtO reduction (peaks 1,2 and 3 from Figure 1) and the theoretical H2 consumption to reduce all the PtO present in the catalyst to Pt0; Table S2: Total acidity (measured by TPD-NH3), and Brønsted to Lewis ratio (measured by FTIR of adsorbed pyridine after vacuum treatment at different temperatures) of supported tungsten oxide materials. Table S3: Textural properties and tungsten surface density of different supported tungsten oxide materials.

Author Contributions: Conceptualization, C.J.-C. and I.G.; methodology, I.A.-T.; formal analysis, C.J.-C. and M.O.B.; data curation, C.J.-C. and M.O.B.; writing—original draft preparation, I.G.; writing—review and editing, P.-L.A.; supervision, I.G.; project administration, I.G. and P.-L.A.; funding acquisition, P.-L.A. All authors have read and agreed to the published version of the manuscript.

Conflicts of Interest: The authors declare no conflict of interest.

References

1. Ruppert, A.M.; Weinberg, K.; Palkovits, R. Hydrogenolysis goes bio: From carbohydrates and sugar alcohols to platform chemicals. *Angew. Chem. Int. Ed.* **2012**, *51*, 2564–2601. [CrossRef]
2. Chen, K.; Koso, S.; Kubota, T.; Nakagawa, Y.; Tomishige, K. Chemoselective Hydrogenolysis of Tetrahydropyran-2-methanol to 1,6-Hexanediol over Rhenium-Modified Carbon-Supported Rhodium Catalysts. *ChemCatChem* **2010**, *2*, 547–555. [CrossRef]
3. Xu, W.; Wang, H.; Liu, X.; Ren, J.; Wang, Y.; Lu, G. Direct catalytic conversion of furfural to 1,5-pentanediol by hydrogenolysis of the furan ring under mild conditions over Pt/Co2AlO4 catalyst. *Chem. Commun.* **2011**, *47*, 3924–3926. [CrossRef]
4. Soghrati, E.; Kok Poh, C.; Du, Y.; Gao, F.; Kawi, S.; Borgna, A. C–O Hydrogenolysis of Tetrahydrofurfuryl Alcohol to 1,5-Pentanediol Over Bi-functional Nickel-Tungsten Catalysts. *ChemCatChem* **2018**, *10*, 4652–4664. [CrossRef]
5. García-Fernández, S.; Gandarias, I.; Requies, J.; Güemez, M.B.; Bennici, S.; Auroux, A.; Arias, P.L. New approaches to the Pt/WOx/Al2O3 catalytic system behavior for the selective glycerol hydrogenolysis to 1,3-propanediol. *J. Catal.* **2015**, *323*, 65–75. [CrossRef]
6. Checa, M.; Nogales-Delgado, S.; Montes, V.; Encinar, J.M. Recent Advances in Glycerol Catalytic Valorization: A Review. *Catalysts* **2020**, *10*, 1279. [CrossRef]
7. Omar, L.; Perret, N.; Daniele, S. Self-Assembled Hybrid ZnO Nanostructures as Supports for Copper-Based Catalysts in the Hydrogenolysis of Glycerol. *Catalysts* **2021**, *11*, 516. [CrossRef]
8. Gandarias, I.; Requies, J.; Arias, P.L.; Armbruster, U.; Martin, A. Liquid-phase glycerol hydrogenolysis by formic acid over Ni-Cu/Al2O3 catalysts. *J. Catal.* **2012**, *290*, 79–89. [CrossRef]
9. Yu, X.; Zhang, F.; Wang, Y.; Cheng, D. Easily Recycled CuMgFe Catalysts Derived from Layered Double Hydroxides for Hydrogenolysis of Glycerol. *Catalysts* **2021**, *11*, 232. [CrossRef]
10. Chia, M.; Pagán-Torres, Y.J.; Hibbitts, D.; Tan, Q.; Pham, H.N.; Datye, A.K.; Neurock, M.; Davis, R.J.; Dumesic, J.A. Selective hydrogenolysis of polyols and cyclic ethers over bifunctional surface sites on rhodium-rhenium catalysts. *J. Am. Chem. Soc.* **2011**, *133*, 12675–12689. [CrossRef]
11. Arundhathi, R.; Mizugaki, T.; Mitsudome, T.; Jitsukawa, K.; Kaneda, K. Highly selective hydrogenolysis of glycerol to 1,3-propanediol over a boehmite-supported platinum/tungsten catalyst. *ChemSusChem* **2013**, *6*, 1345–1347. [CrossRef]
12. Zhao, B.; Liang, Y.; Liu, L.; He, Q.; Dong, J.-X. Facilitating Pt–WOx Species Interaction for Efficient Glycerol Hydrogenolysis to 1,3-Propanediol. *ChemCatChem* **2021**, *13*, 3695–3705. [CrossRef]

13. Xi, Z.; Hong, Z.; Huang, F.; Zhu, Z.; Jia, W.; Li, J. Hydrogenolysis of Glycerol on the ZrO2-TiO2 Supported Pt-WOx Catalyst. *Catalysts* **2020**, *10*, 312. [CrossRef]

14. Aihara, T.; Kobayashi, H.; Feng, S.; Miura, H.; Shishido, T. Effect of WO_3 loading on the activity of $Pt/WO_3/Al_2O_3$ catalysts in selective hydrogenolysis of glycerol to 1,3-propanediol. *Chem. Lett.* **2017**, *46*, 1497–1500. [CrossRef]

15. García-Fernández, S.; Gandarias, I.; Tejido-Núñez, Y.; Requies, J.; Arias, P.L. Influence of the Support of Bimetallic Platinum Tungstate Catalysts on 1,3-Propanediol Formation from Glycerol. *ChemCatChem* **2017**, *9*, 4508–4519. [CrossRef]

16. Zhou, W.; Luo, J.; Wang, Y.; Liu, J.; Zhao, Y.; Wang, S.; Ma, X. WOx domain size, acid properties and mechanistic aspects of glycerol hydrogenolysis over $Pt/WO_x/ZrO_2$. *Appl. Catal. B Environ.* **2019**, *242*, 410–421. [CrossRef]

17. Zhu, S.; Gao, X.; Zhu, Y.; Cui, J.; Zheng, H.; Li, Y. SiO_2 promoted $Pt/WO_x/ZrO_2$ catalysts for the selective hydrogenolysis of glycerol to 1,3-propanediol. *Appl. Catal. B Environ.* **2014**, *158–159*, 391–399. [CrossRef]

18. Zhu, S.; Gao, X.; Zhu, Y.; Li, Y. Chemical Promoting effect of WO_x on selective hydrogenolysis of glycerol to 1,3-propanediol over bifunctional $Pt–WO_x/Al_2O_3$ catalysts. *J. Mol. Catal. A Chem.* **2015**, *398*, 391–398. [CrossRef]

19. Zhu, M.; Chen, C. Hydrogenolysis of glycerol to 1,3-propanediol over $Li_2B_4O_7$-modified tungsten–zirconium composite oxides supported platinum catalyst. *React. Kinet. Mech. Catal.* **2018**, *124*, 683–699. [CrossRef]

20. Barton, D.; Soled, S.L.; Meitzner, G.D.; Fuentes, G.A.; Iglesia, E. Structural and Catalytic Characterization of Solid Acids Based on Zirconia Modified by Tungsten Oxide. *J. Catal.* **1999**, *181*, 57–72. [CrossRef]

21. Mohamedkhair, A.K.; Drmosh, Q.A.; Qamar, M.; Yamani, Z. Tuning Structural Properties of WO_3 Thin Films for Photoelectrocatalytic Water Oxidation. *Catalysts* **2021**, *11*, 381. [CrossRef]

22. Jelinska, A.; Bienkowski, K.; Jadwiszczak, M.; Pisarek, M.; Strawski, M.; Kurzydlowski, D.; Solarska, R.; Augustynski, J. Enhanced Photocatalytic Water Splitting on Very Thin WO_3 Films Activated by High-Temperature Annealing. *ACS Catal.* **2018**, *8*, 10573–10580. [CrossRef]

23. Brunelle, J.P. Preparation of Catalysts by Adsorption of Metal Complexes on Mineral Oxides. *Pure Appl. Chem.* **1979**, *3*, 211–232.

24. Mulcahy, F.M.; Houalla, M.; Hercules, D.M. The effect of the isoelectric point on the adsorption of molybdates on fluoride-modified aluminas. *J. Catal.* **1987**, *106*, 210–215. [CrossRef]

25. Kohler, S.D.; Ekerdt, J.G.; Kim, D.S.; Wachs, I.E. Relationship between structure and point of zero surface charge for molybdenum and tungsten oxides supported on alumina. *Catal. Lett.* **1992**, *16*, 231–239. [CrossRef]

26. Hao, X.; Quach, L.; Korah, J.; Spieker, W.A.; Regalbuto, J.R. The control of platinum impregnation by PZC alteration of oxides and carbon. *J. Mol. Catal. A Chem.* **2004**, *219*, 97–107. [CrossRef]

27. Shyu, J.Z.; Otto, K. Identification of platinum phases on γ-alumina by XPS. *Appl. Surf. Sci.* **1988**, *32*, 246–252. [CrossRef]

28. Wu, X.; Zhang, L.; Weng, D.; Liu, S.; Si, Z.; Fan, J. Total oxidation of propane on $Pt/WO_x/Al_2O_3$ catalysts by formation of metastable Pt^+ species interacted with WO_x clusters. *J. Hazard. Mater.* **2012**, *225*, 146–154. [CrossRef] [PubMed]

29. Vermaire, D.C.; van Berge, P.C. The preparation of WO_3TiO_2 and $WO_3Al_2O_3$ and characterization by temperature-programmed reduction. *J. Catal.* **1989**, *116*, 309–317. [CrossRef]

30. Cruz, J.; Avalos-Borja, M.; López Cordero, R.; Bañares, M.A.; Fierro, J.L.G.; Palacios, J.M.; López Agudo, A. Influence of pH of the impregnation solution on the phosphorus promotion in W/Al_2O_3 hydrotreating catalysts. *Appl. Catal. A Gen.* **2002**, *224*, 97–110. [CrossRef]

31. Pope, M.T. *Heteropoly and Isopoly Oxometalates*; Springer: Berlin/Heidelberg, Germany, 1983.

32. Barton, D.G.; Shtein, M.; Wilson, R.D.; Soled, S.L.; Iglesia, E. Structure and Electronic Properties of Solid Acids Based on Tungsten Oxide Nanostructures. *J. Phys. Chem. B* **1999**, *103*, 630–640. [CrossRef]

33. Wachs, I.E.; Kim, T.; Ross, E.I. Catalysis science of the solid acidity of model supported tungsten oxide catalysts. *Catal. Today* **2006**, *116*, 162–168. [CrossRef]

34. Kwak, J.H.; Hu, J.; Mei, D.; Yi, C.-W.; Kim, D.H.; Peden, C.H.F.; Allard, L.F.; Szanyi, J. Coordinatively Unsaturated Al^{3+} Centers as Binding Sites for Active Catalyst Phases of Platinum on g-Al_2O_3. *Science* **2009**, *325*, 1670–1674. [CrossRef]

35. Knözinger, H. Infrared Spectroscopy for the Characterization of Surface Acidity and Basicity. In *Handbook of Heterogeneous Catalysis*, 2nd ed.; Ertl, G., Knözinger, H., Schüth, F., Weitkamp, J., Eds.; Wiley-VCH: Weinheim, Germany, 2008.

36. Aihara, T.; Miura, H.; Shishido, T. Effect of perimeter interface length between 2D WO_3 monolayer domain and γ-Al_2O_3 on selective hydrogenolysis of glycerol to 1,3-propanediol. *Catal. Sci. Technol.* **2019**, *9*, 5359–5367. [CrossRef]

37. Amada, Y.; Shinmi, Y.; Koso, S.; Kubota, T.; Nakagawa, Y.; Tomishige, K. Reaction mechanism of the glycerol hydrogenolysis to 1,3-propanediol over Ir-ReO_x/SiO_2 catalyst. *Appl. Catal. B Environ.* **2011**, *105*, 117–127. [CrossRef]